Environmental Science and Pollution Research (2023) 30:106585–106597
https://doi.org/10.1007/s11356-023-29879-7

RESEARCH ARTICLE

Use of Co_3O_4 nanoparticles with different surface morphologies for removal of toxic substances and investigation of antimicrobial activities via in vivo studies

Nurdan Kurnaz Yetim[1] · Elvan Hasanoğlu Özkan[2] · Hatice Öğütçü[3]

Received: 25 June 2023 / Accepted: 10 September 2023 / Published online: 21 September 2023

Abstract

Co_3O_4 nanoparticles (NPs) were formed using hydrothermal synthesis method and various surfactants to study the effect of changing surface morphology on catalytic and antibacterial activities. FT-IR, TEM, SEM, BET, XRD, and XPS analyses were performed to characterize the NPs. It was observed that as the morphology of Co_3O_4 changes, it creates differences in the reduction efficiency of organic dyes and p-nitrophenol (p-NP), which are toxic to living organisms and widely used in industry. The reaction rate constants (K_{app}) for Co_3O_4-urea, Co_3O_4-ed, and Co_3O_4-NaOH in the reduction of p-NP were found to be 1.86×10^{-2} s^{-1}, 1.83×10^{-2} s^{-1}, and 2.4×10^{-3} s^{-1}, respectively. In the presence of Co_3O_4-urea catalyst from the prepared nanoparticles, 99.29% conversion to p-aminophenol (p-AP) was observed, while in the presence of the same catalyst, 98.06% of methylene blue (MB) was removed within 1 h. The antibacterial activity of Co_3O_4 particles was compared with five standard antibiotics for both gram-positive and gram-negative bacteria. The results obtained indicate that the antimicrobial activity of the synthesized Co_3O_4 particles has a remarkable inhibitory effect on the growth of various pathogenic microorganisms. The current work could be an innovative and beneficial search for both biomedical and wastewater treatment applications.

Keywords Hydrothermal synthesis · Co_3O_4 · Methylene blue · p-NP · Antimicrobial activity

Introduction

Nitroaromatic compounds and/or organic dyes are substances that have toxic properties for humans, animals, and plants but are widely used in industry (Muhammad et al. 2019; Najafabadi et al. 2022; Nava et al. 2022). Their removal is essential for the protection of the health of living organisms and can be achieved through adsorption, advanced oxidation processes, chemical reduction, and aerobic biodegradation (Fast et al. 2017). Chemical reduction is an important and inexpensive method for the extraction of nitroaromatics and azo dyes by converting hydrogen into relatively low-toxicity products that can be easily degraded in nature (Li et al. 2021a, b; Rahman and Jonnalagadda 2008). High surface area activated carbon, and microalgae have been used as catalysts by many researchers to achieve high degradation performance towards organic pollutants (Mohd Hanafi et al. 2022; Jasri et al. 2023; Abdulhameed et al. 2022; Nadhirah Long Tamjid Farki NNA 2023). Razali et al. synthesized high surface area activated carbon (MSMPAC) using mixed fruit waste from mango (*Mangifera indica*) seeds (MS) and peels (MP), microwave-induced $ZnCl_2$ activation and evaluated it for the removal of methylene blue (MB) from an aqueous medium (Razali et al. 2022). On the other hand, most of the metal-based catalysts for this hydrogenation reaction of nitroaromatic compounds heavily depend on noble metals (Li et al. 2021a, b; Zaera 2017; Kim et al. 2022). Most of the catalytic reactions in the noble metal nanoparticles (NP) take place only on the surface of the nitroaromatic compounds, and most of the atoms in the

Responsible Editor: Guilherme Luiz Dotto.

✉ Elvan Hasanoğlu Özkan
ehasanoglu@gazi.edu.tr

[1] Department of Chemistry, Faculty of Arts and Sciences, University of Kırklareli, Kırklareli, Turkey

[2] Department of Chemistry, Faculty of Science, Gazi University, Teknikokullar, 06500 Ankara, Turkey

[3] Department of Field Corps, Faculty of Agriculture, University of Kırşehir Ahi Evran, Kırşehir, Turkey

nucleus are catalytically inactive (Seitkalieva et al. 2021; Mohanty et al. 2010). However, the process is not financially friendly, and this reduces its areas of use. For this reason, to generate a large percentage of the noble metal atoms accessible for catalysis and to reduce their use, the internal noble metal atoms must be replaced by non-noble metals such as iron (Fe), cobalt (Co), and nickel (Ni) (Badruzzaman et al. 2020; Karimi et al. 2021; Ryabchuk et al. 2018). As an alternative, heterogeneous catalysts produced using non-precious metals, hydroxides, and oxides have gained importance due to their superior attributes with substantially more feasible costs compared to noble metals (Singh et al. 2017; Kurnaz Yetim et al. 2022; Wang et al. 2015; Ozkan 2023; Wen et al. 2018). Making a comparison with non-precious metals with higher oxidizing properties, and with challenging production procedures, oxide metals show similar reaction properties, superior chemical stability, and easier production aspects (Zhang et al. 2021). For this reason, non-precious metal oxides are one of the most commonly used functional materials for various catalytic implementations (Naseem et al. 2021; Danish et al. 2020; Gebre and Sendeku 2019).

The transition of cobalt oxide is of significant importance thanks to its electrical, optical, and magnetic properties (Prakash et al. 2022; Anuma et al. 2021; Ambika et al. 2019). Cobalt possesses Co^{4+}, Co^{3+}, and Co^{2+} oxidation steps. For this reason, it exists in the forms of cobalt (II) oxide (CoO), cobalt (III) oxide (Co_2O_3), and cobalt (II, III) oxide (Co_3O_4). The Co_3O_4 phase is the most commonly seen of these forms. Co_3O_4 is highly stable in terms of chemical activity and possesses rich redox reactivity in numerous reactions (Liu et al. 2022; Xu et al. 2022; Cheng et al. 2021). Size, shape, surface area, crystallinity, defects, and surface oxidation state are the important parameters that affect the catalytic activity of Co_3O_4. In previous studies, various approaches were adopted including size and pore modulation, ion doping, surface defect generation, and support-induced interactions to modify mass transfer and electron transfer that increase the catalytic activities of Co_3O_4 nanoparticles in chemical reduction reactions (Zhang et al. 2017; Mogudi et al. 2016).

In the last 10 years, inorganic nanoparticles (NPs) with unique physical, chemical, and biological properties have become of particular importance against bacterial infections (Khan et al. 2019; Jeevanandam et al. 2018). In general, organic antimicrobial agents have lower stability, especially at high temperatures or pressures, and can be seriously harmful and/or toxic. On the other hand, inorganic materials with antibacterial properties including inorganic metal oxides are rigid and ductile. Their superior properties over organic antimicrobial agents include stability, rigidness, and chemical stability over a longer time (Pugazhendhi et al. 2021). In addition, metal oxide NPs replace the most frequently used silver oxides, which due to their toxicity have adverse effects on humans and the surrounding environment (Kavitha et al. 2017).

Various Co_3O_4 with different morphologies have been reported in the literature. These have shown various catalytic performances based on their surface area, surfactant species, reducibility, and morphology (Chiu et al. 2020; Din et al. 2021; Xu et al. 2022). Therefore, it will be necessary to investigate Co_3O_4 with various morphologies, especially nanostructures, to offer insights towards optimizing Co_3O_4 design to investigate the morphology-based catalytic reactivity and antimicrobial effect of Co_3O_4 catalysts. Therefore, the aim of this work is to investigate Co_3O_4 catalysts with various nanostructured morphologies for p-NP reduction.

In this study, Co_3O_4 structures with three different morphologies were obtained by using the hydrothermal synthesis method (Kurnaz Yetim 2021). The effect of the morphology of the Co_3O_4 NPs produced on the catalytic and antimicrobial properties against pathogenic strains (Gram (−) and Gram (+) bacteria and yeast) were examined (see Fig. 1).

Materials and methods

Spectral data measurements

A Rigaku MiniFlex 600 X-ray diffractometer equipped with a Ni-filtered Cu Kα source was utilized to determine the X-ray diffraction (XRD) patterns over a scan range of $10° < 2\theta < 90°$. The infrared spectrum was recorded using a Jasco FT-IR-6700 spectrometer, and the wavelength range was between 400 and 4000 cm^{-1}. In addition, scanning electron microscopy (SEM) was utilized to examine the surface morphology of the Co_3O_4 structures. Energy dispersive x-ray spectroscopy (EDX) was adopted for the determination of the elemental composition of the Co_3O_4 structures. A FEI Quanta 400F model device was utilized for the SEM–EDX analyses. Brunauer–Emmett–Teller (BET) analysis was performed to examine the surface area of the nanostructures. Quantachrome-Nova Touch LX^4 instrument was used for this purpose.

Synthesis of the Co_3O_4 structures

The synthesis of Co_3O_4-urea, Co_3O_4-ed, and Co_3O_4-NaOH structures was carried out following the procedure in the previous research (Kurnaz Yetim 2021). In Fig. 2, the synthesis scheme of Co_3O_4 nanoparticles is presented.

Co_3O_4-urea was prepared by dissolving 1.45 g of $Co(NO_3)_2{\cdot}6H_2O$ and 1.5 g $CO(NH_2)_2$ in 40 mL of water under stirring for 30 min, and a homogeneous solution was obtained. The resulting mixture was placed into a

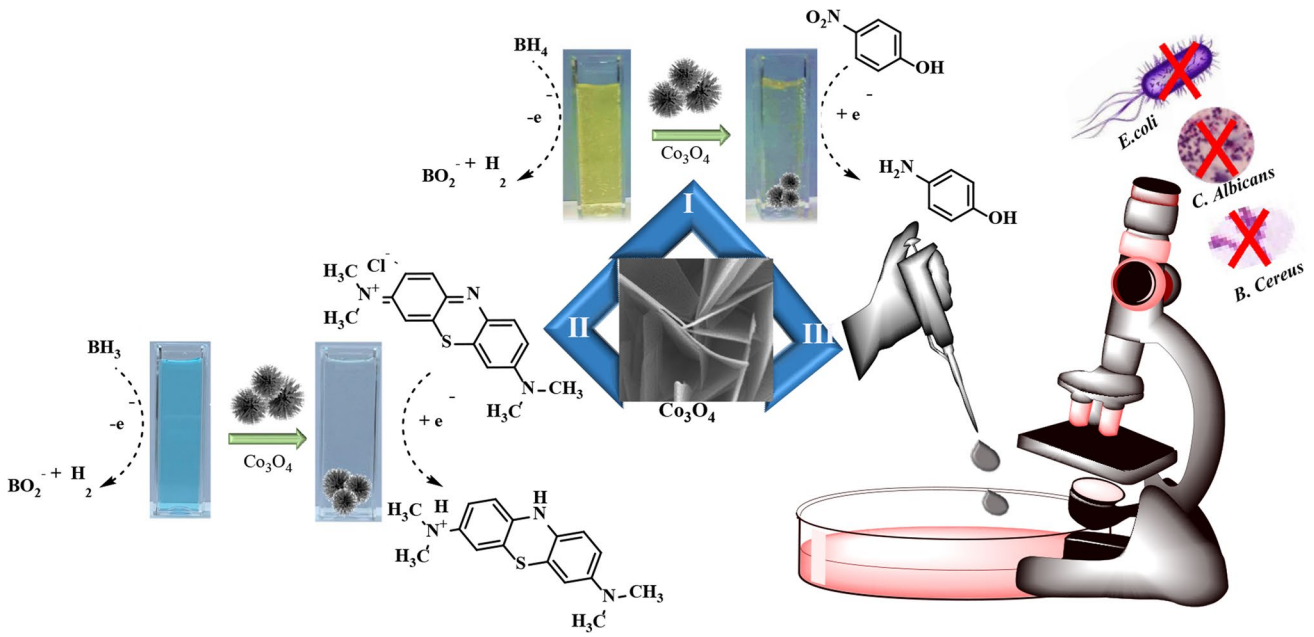

Fig. 1 Schematic representation of the catalysis reaction mechanism and antimicrobial properties of Co_3O_4 nanoparticles

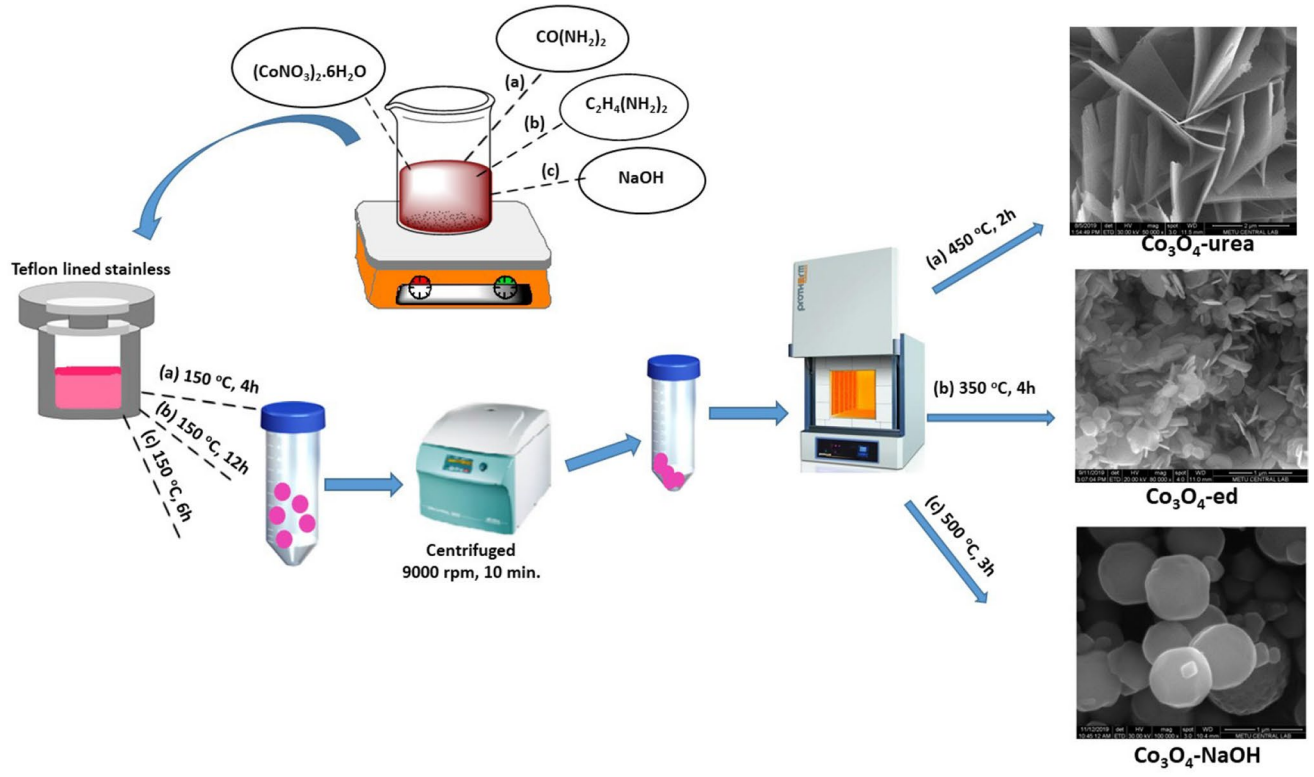

Fig. 2 Synthesis scheme of Co_3O_4 nanoparticles obtained using different surfactants

Teflon-lined stainless steel autoclave with a capacity of 50 mL, autoclaved in an oven at 150 °C for 4 h. The precipitate was rinsed with distilled water and ethanol and dried at 80 °C for 24 h. Finally, the product was left to anneal at 450 °C in the air for 2 h under ambient conditions at a rate of 10 °C/min.

To obtain Co_3O_4-ed, 1.45 g of $Co(NO_3)_2{\cdot}6H_2O$ was dissolved in 25 mL of water and then 0.5 mL of ethylenediamine was added. The pH was adjusted to 12 using 2 M of NaOH. The solution was stirred for 30 min, and the mixture was transferred to a 50-mL capacity Teflon-lined stainless steel autoclave. The solution in the autoclave was then placed in an oven and autoclaved 150 °C for 12 h. The solution was cooled to room temperature, and the precipitate was rinsed with distilled water and ethanol, and then left to dry at 60 °C for 12 h. Finally, the product was left to anneal at 350 °C in the air for 2 h at a rate of 10 °C/min.

To obtain Co_3O_4-NaOH, 5.82 g of $Co(NO_3)_2{\cdot}6H_2O$ and 0.2 g of sodium hydroxide were dissolved in deionized water (10 mL) under vigorous stirring for 10 min. The solution was then transferred in a Teflon-lined stainless steel autoclave of 50 mL capacity and autoclaved at 150 °C for 6 h. The solution was cooled to room temperature, and the precipitate was rinsed with distilled water and ethanol, and then left to dry at 60 °C for 10 h. Finally, the product was left to anneal at 500 °C in the air for 3 h at a rate of 10 °C/min.

Reduction of p-NP and MB

Catalysis studies were conducted by observing the conversion of p-NP molecules into p-AP molecules by Co_3O_4 NM-based catalysis. In this procedure, $NaBH_4$ was utilized as the hydrogen source. Accordingly, approximately 3-mg Co_3O_4 flower-like particles were placed into a 3-mL solution containing 0.1 mM of p-NP and 0.3 mL of 0.2 M $NaBH_4$. The concentration of the p-NP and p-AP was examined utilizing a spectrophotometric method (Kurnaz Yetim and Hasanoğlu Ozkan 2021).

To realize a reduction study, approximately 3 mg of Co_3O_4 NPs was placed in 4 mL of a 7.5 mg/L MB aqueous solution, then 0.3 mL of fresh $NaBH_4$ aqueous solution was added. The resulting mixture was then examined by measuring the absorbance of the solution at 664-nm wavelength at different periods to examine the concentration of the remaining MB solution (Erdogan 2020).

Analysis of the antimicrobial potential of Co_3O_4 NPs

Detection of antimicrobial activity

The antibacterial activity of Co_3O_4 NPs was tested against the six Gram-negative bacteria (*Salmonella typhi*, *Escherichia coli*, *Enterobacter aerogenes* sp., *Klebsiella pneumoniae*, *Proteus vulgaris*, and *Pseudomonas aeruginosa*), five Gram-positive bacteria (*Staphylococcus aureus*, *Staphylococcus epidermis*, *Micrococcus luteus*, *Bacillus cereus*, and *Listeria monocytogenes*), and one yeast (*Candida albicans*) by the Agar well diffusion assay method. The NPs were kept dry at room temperature and dissolved (100 µg/mL and 200 µg/mL) in DMSO. DMSO was utilized as the solvent for the compound and the control. It was determined that DMSO had no antimicrobial activity against any of the pathogenic microorganisms. A 1% (v/v) 24-h broth culture (pathogenic bacteria and yeast) containing 10^6 cfu/mL was placed on a sterile plate. Mueller–Hinton Agar (MHA) (15 mL) at 45 °C was poured into Petri dishes and left to cool and solidify. Then, 6-mm-diameter wells were carefully drilled utilizing a sterile cork drill and filled with the synthesized NPs and incubated for 24 h at 37 °C (Ogutcu et al. 2017). At the end of incubation, the average of the two wells was utilized to calculate the growth inhibition zone of each pathogenic bacteria and yeast (to compare the degree of inhibition, bacteria and yeast were tested for resistance to four antibiotics (kanamycin, ampicillin, amoxicillin, and sulfamethoxazole) and one anticandidal (nystatin) (Anar et al. 2016).

Results and discussion

Characterization of Co_3O_4 NPs

FT-IR, XRD, and XPS analyses of Co_3O_4 NPs are given in the Supporting Information (Kurnaz Yetim 2021). The SEM images of the Co_3O_4 samples prepared using different ligands are given in Fig. 3. The figure shows the morphological and structural properties of the Co_3O_4 structures.

Figure 3(a) presents the Co_3O_4-urea in the nanosheet form. The expanded figure shown in Fig. 3(d) was prepared to identify the well-assembled multi-layered microplates in porous form. Figure 3 (b) shows the Co_3O_4-ed sample. This sample was in a clover leaf-like form; the accumulation of small clover-like formations can be seen. The size of the clover-like formations was in the range of 500–1000 nm. SEM images of Co_3O_4-NaOH sample are shown in Fig. 3(e) and (f). SEM images of Co_3O_4-NaOH show that the structure is in the form of nanospheres. The size distribution of the nanospheres was narrow, and the average size was approximately 700 nm.

The surface properties of Co_3O_4 catalysts were investigated by N_2 gas adsorption–desorption method at 77 K. Surface areas were calculated according to Brunauer–Emmett–Teller (BET) method, and pore volume distribution was calculated according to Barrett-Joyner-Halenda (BJH) method using adsorption analysis, and isotherms are presented in Fig. 4. When the N_2 adsorption–desorption isotherms of metal oxides were examined, the characteristic of mesoporous materials containing hysteresis loop suggested that the isotherms classified as type IV according to IUPAC. The specific surface area of the samples was calculated by BET method and found to be 146.185 m^2/g, 106.506 m^2/g, and 31.0885 m^2/g for Co_3O_4-urea, Co_3O_4-ed, and Co_3O_4-NaOH, respectively. The average

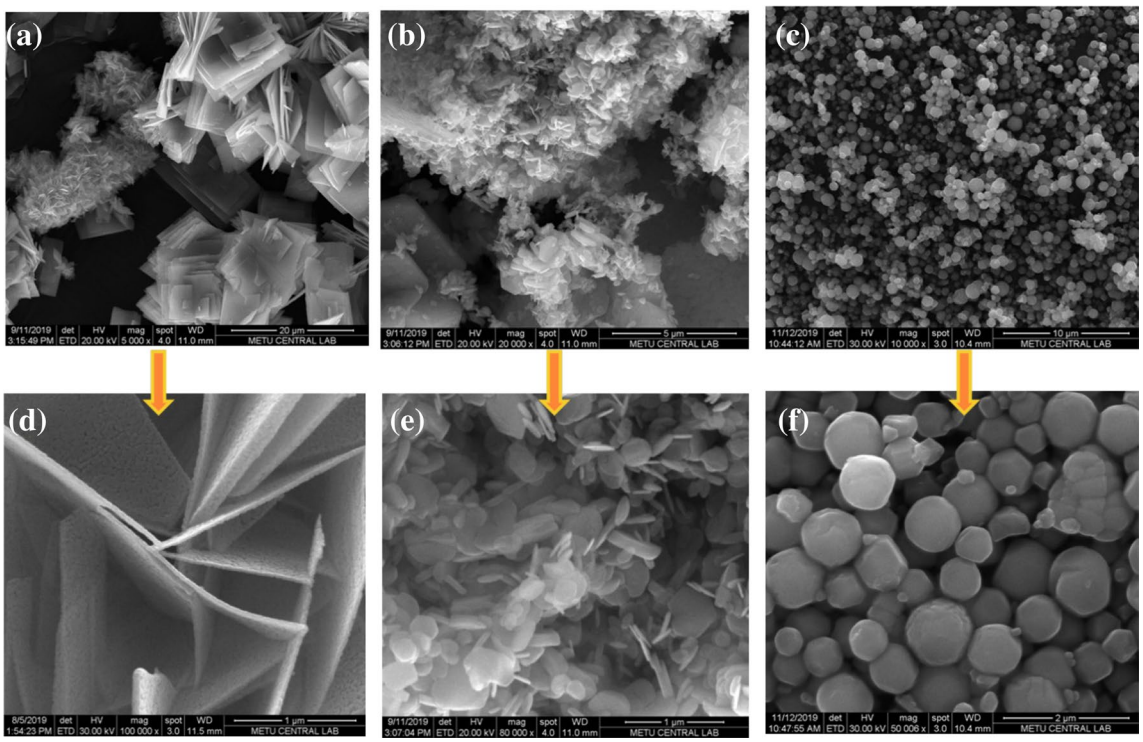

Fig. 3 The SEM images of (a) Co_3O_4–urea, (b) Co_3O_4-ed, (c) Co_3O_4-NaOH and corresponding magnified SEM images (d), (e), and (f)

pore diameter of the produced Co3O4 NPs was found to be 3.48978 nm, 3.6477 nm, and 2.5318 nm for Co_3O_4-urea, Co_3O_4-ed, and Co_3O_4-NaOH, respectively. The measured surface areas of Co_3O_4 nanoflowers were in line with the results reported in previous studies, which were 34.61 m^2/g and 51.2 m^2/g (Zhang et al. 2008; Sun et al. 2013). When compared with the literature data, it is seen that Co_3O_4 structures have a very large surface area. When the rate constants for the reduction reaction of p-NP are examined, it can be said that the surface areas of the catalysts used are parallel to the reaction rate.

Catalytic activity

Catalytic degradation of p-NP

The reduction process of p-NP to p-AP involves both electron transfer and hydrogen transport. It is widely known that negative hydride species (H^-) obtained from BH_4^- anions present electrons and hydrogen atoms. This study investigated the catalytic activities of synthesized Co_3O_4 NPs with different morphologies partaking in the process of reducing p-NP to p-AP in the presence of $NaBH_4$. The catalytic activities of noble metals and metal oxides in this reaction have been frequently studied (Najafi and Azizian 2020). However, there are very few studies on the effect of morphology on catalytic activity in this reduction process (Ye et al. 2021; Liu et al. 2021). For all experiments, p-NP and $NaBH_4$ were reacted together with initial concentrations of 0.1 mM and 0.2 M, respectively. The p-NP bound peak observed at a wavelength of 317 nm in the UV–Vis spectra shifted immediately to 400 nm after the addition of the freshly prepared $NaBH_4$ solution. This peak is due to the formation of the p-nitrophenolate ion in the alkaline state caused by the addition of $NaBH_4$. The simultaneous appearance of a new peak around 295 to 300 nm, with the addition of Co_3O_4-urea, Co_3O_4-ed, and Co_3O_4-NaOH, resulted in reduced absorption of the characteristic peak at a wavelength of 400 nm that confirmed the formation of p-AP. The time taken to complete the conversion varied depending on the morphology of the catalyst.

In the absence of the catalyst, conversion of the p-NP solution to p-AP takes up to 4 to 5 h. When 3 mg of Co_3O_4 catalyst was added to the medium, it was observed that this conversion took place in 4 to 5 min. Therefore, it appears that the less efficient electron and hydrogen transfer from the BH_4^- species to the aromatic nitro compound without a catalyst increases significantly in the presence of metal oxides. Table 1 summarizes the activity of metal oxides and the variation of the reduction reaction according to the amount of catalyst. The reaction rate constants (K_{app}) for Co_3O_4-urea, Co_3O_4-ed, and Co_3O_4-NaOH in the reduction of p-NP were found to be 1.86×10^{-2} s^{-1}, 1.83×10^{-2} s^{-1}, and 2.4×10^{-3} s^{-1}, respectively. These results indicate that

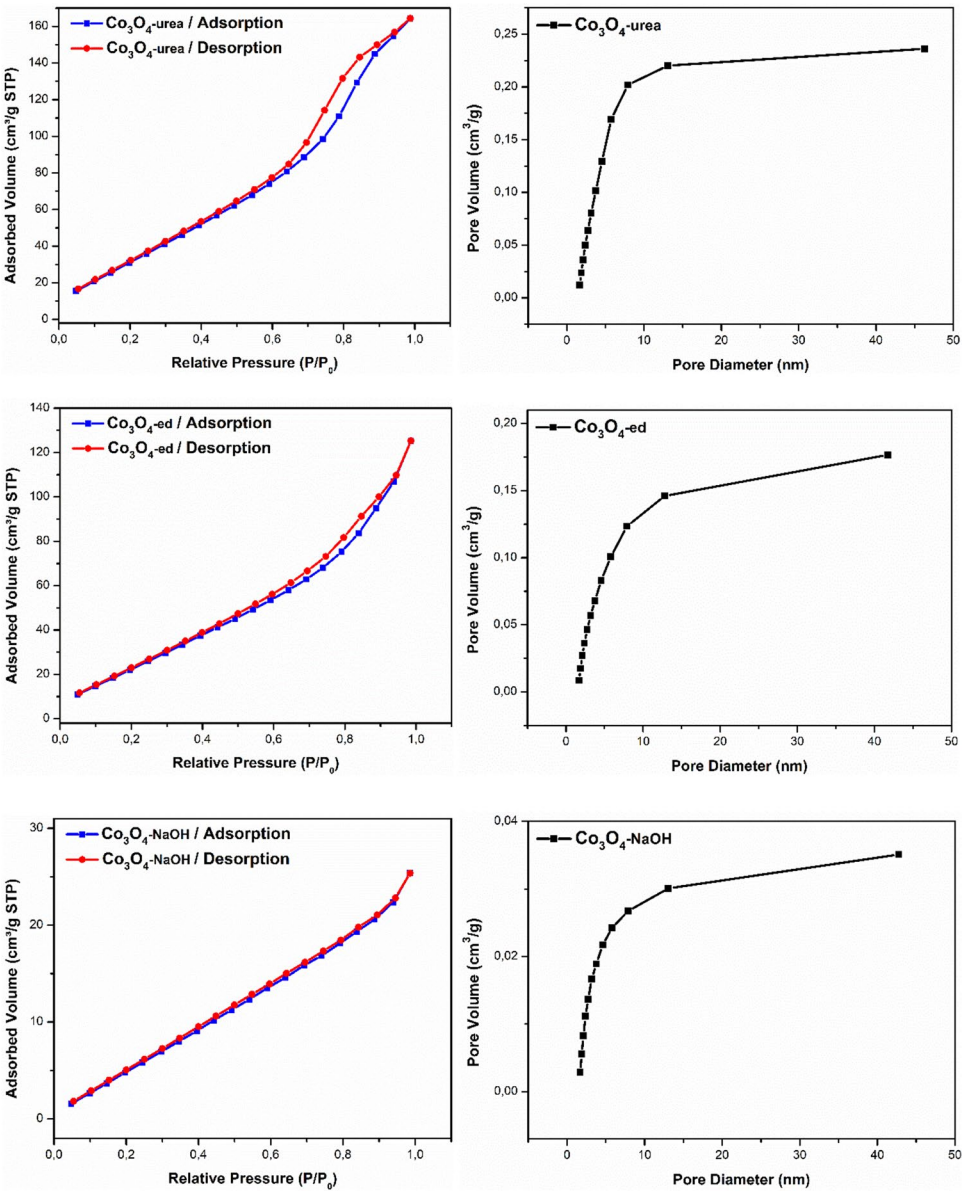

Fig. 4 BET analysis and pore size distribution of Co_3O_4 nanostructures

Table 1 Reduction results of p-NP in the presence of Co_3O_4 nanoparticles and nanocomposites in literature

Catalyst	Amount of catalyst	Time	K_{app}	Ref
Co_3O_4-urea	3 mg	270 s	1.86×10^{-2} s^{-1}	Present study
Co_3O_4-ed	3 mg	300 s	1.83×10^{-2} s^{-1}	Present study
Co_3O_4-NaOH	3 mg	330 s	2.4×10^{-3} s^{-1}	Present study
Conical-Co_3O_4	0.063 mL	5.64 min	0.6882 min^{-1}	Chiu et al. (2020)
Stacked-Co_3O_4	(1 mg/mL)	6.87 min	0.4928 min^{-1}	
Needled-Co_3O_4		6.28 min	0.6171 min^{-1}	
Floral-Co_3O_4		8.24 min	0.4709 min^{-1}	
Reduced Co_3O_4	0.1 mL (0.071 mg/mL)	7.25 min	1.49 min^{-1}	Chen et al. (2017)
rGO-Co_3O_4	100 mL (0.5 mg/mL)	60 s	-	Nafiey et al. (2017)
Co_3O_4/HNTs	0.1 mg	11 min	0.265 min^{-1}	Zhang et al. (2021)
Co_3O_4	3 mg	20 min	2.2×10^{-3} s^{-1}	Hasanoğlu Ozkan et al. (2022)
Co/CoO	3 mg	12 min	0.0404	Din et al. (2021)

all three catalysts can successfully catalyze the reduction reaction (see Fig. 5).

Catalytic degradation of MB

The catalytic degradation of MB was carried out in the presence of Co_3O_4 NPs. MB absorbs strongly at a wavelength of 664 nm in the visible region and gives a deep blue color upon the addition of aqueous $NaBH_4$. Time-dependent UV–Vis spectra of MB reduction are presented in Fig. 6a–c. Absorption spectra were recorded every 5 min. In the presence of Co_3O_4-urea catalyst, 98.06% degradation of MB was observed within 60 min. Time-dependent UV–Vis absorption spectra exhibited that the intensity of the absorption peak of the dyes gradually decreased in the presence of Co_3O_4, disappearing over time. Also, the position of the absorption peak did not noticeably vary throughout the reduction. Furthermore, the degradation kinetics of MB by $NaBH_4$ in the presence of Co_3O_4 NPs was examined by pseudo-first-order kinetics. Figure 6 d shows the linear relationship between $ln\,(C_t/C_0)$ and reaction time. Also, the reaction rate constants were calculated from the slopes.

The reaction rate constants (K_{app}) for Co_3O_4-urea, Co_3O_4-ed, and Co_3O_4-NaOH in the reduction of MB were found to be 6.0×10^{-4} s^{-1}, 2.0×10^{-4} s^{-1}, and 3.0×10^{-4} s^{-1}, respectively (see Table 2).

Antibacterial activity

The NPs considered showed variable growth activity (11 to 22 mm) for the pathogenic microorganisms used, and the activity mainly differed between moderate to high in Fig. 7 which shows images of the antimicrobial effectivity of Co_3O_4 NPs. Furthermore, NPs were more effective on Gram-negative bacteria than Gram-positive bacteria. Antimicrobial activity data shown in Table 3 are as follows.

Co_3O_4-urea showed high activity against *B. cereus*, *E. coli*, and *C. albicans*. In addition, this compound showed the same inhibitory effect as AMC30 (20 mm) for *B. cereus* (Fig. 8). This bacterium is known as an opportunist pathogen and is associated with food-borne illness (Nartop et al. 2019; Nartop et al. 2020a, b). Co_3O_4-ed showed high inhibitory activity against *B. cereus*, *K.*

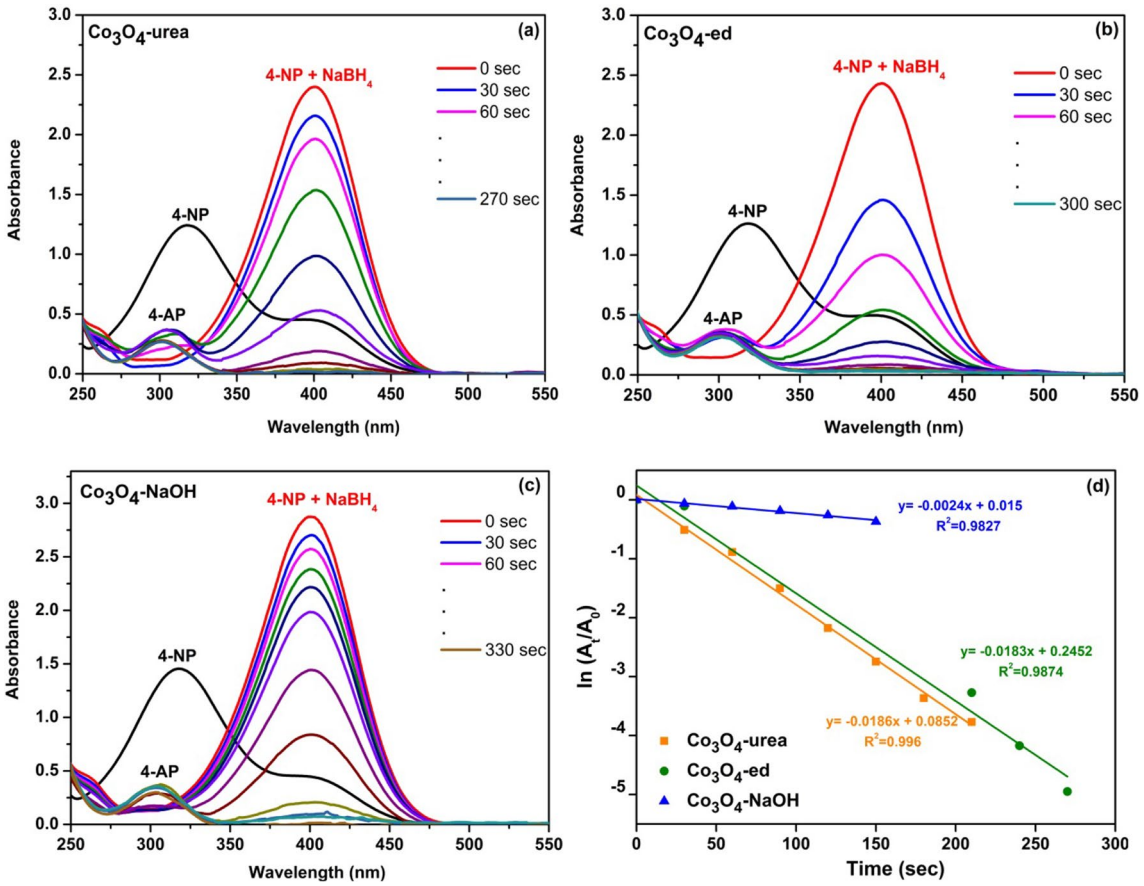

Fig. 5 UV–Vis spectra obtained from the p-NP reduction in the presence of **a** Co_3O_4-urea, **b** Co_3O_4-ed, and **c** Co_3O_4-NaOH nanostructures and **d** the rate constants of the reaction

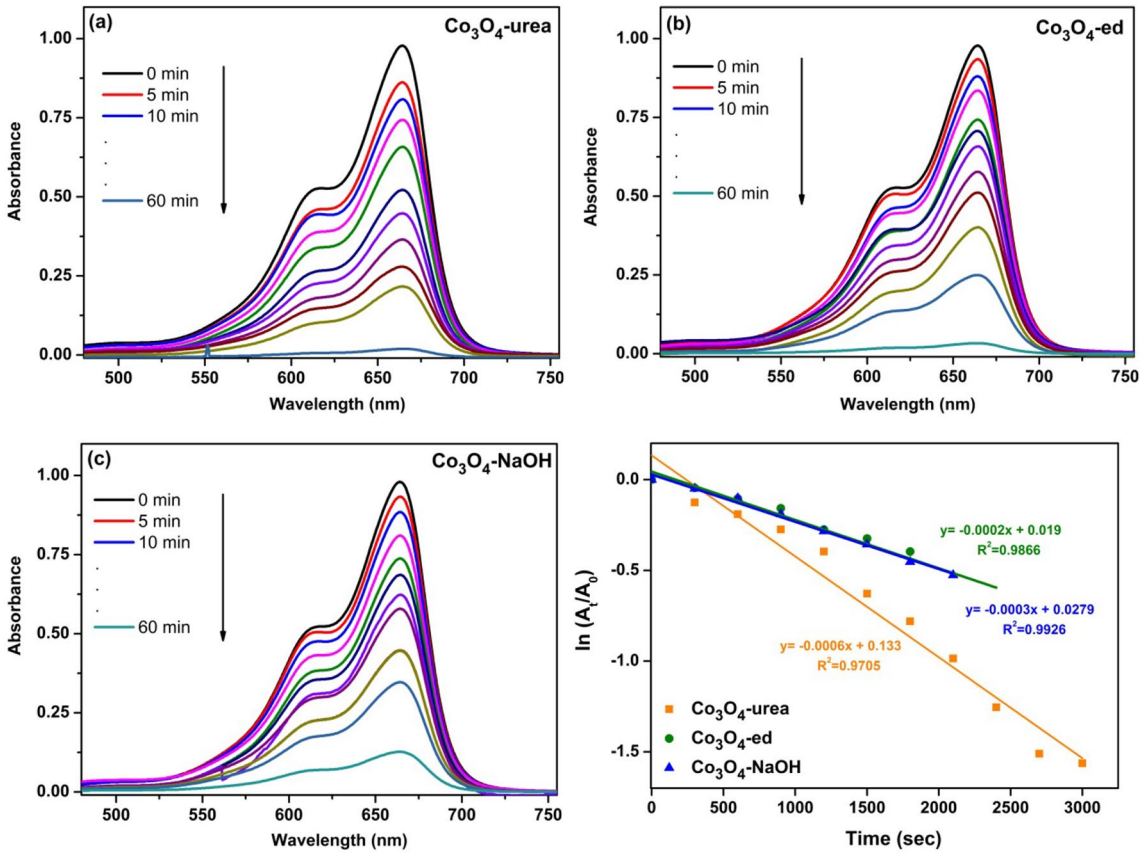

Fig. 6 UV–Vis spectra obtained in the catalytic degradation of MB in the presence of Co_3O_4-urea (**a**), Co_3O_4-ed (**b**), and Co_3O_4-NaOH (**c**), and the rate constants for the reaction (**d**)

Table 2 Reduction results of MB in the presence of Co_3O_4 nanoparticles and different nanocomposites in literature

Catalyst	Amount of catalyst	K_{app}	Ref
Co_3O_4-urea	3 mg	6.0×10^{-4} s^{-1}	Present study
Co_3O_4-ed	3 mg	2.0×10^{-4} s^{-1}	Present study
Co_3O_4-NaOH	3 mg	3.0×10^{-4} s^{-1}	Present study
Co_3O_4/HNTs	0.5 mg	0.155 min^{-1}	Zhang et al. (2021)
AS-AgNPs	0.05 mL	0.7×10^{-3} s^{-1}	Rajasekar et al. (2021)
Fe_3O_4/GO/Ag	0.01 mL	0.2891 min^{-1}	He et al. (2022)
PDOP-FF	1.5 mg	1.4×10^{-3} s^{-1}	Erdogan (2020)
Co/CoO	3 mg	0.042 min^{-1}	Din et al. (2021)

pneumoniae, and *C. albicans* (Fig. 8). Co_3O_4-NaOH exhibited high antimicrobial activity against *B. cereus*, *E. coli*, and *C. albicans*. All three NPs showed a greater inhibitory effect than AMP10 (11 mm) against Gram-negative *S. typhi* (Co_3O_4-urea, Co_3O_4-ed, and Co_3O_4-NaOH, respectively: 13 mm, 13 mm, and 14 mm) (Fig. 8). *Salmonella serovars* lead to many different clinical symptoms including those related to asymptomatic infections, severe typhoid-like syndromes in infants, or some high-sensitivity animals (Koçoğlu et al. 2021; Nartop et al. 2020a, b). In addition, all three NPs showed higher inhibitory activity against *E. coli* than AMP10 (10 mm) and AMC30 (14 mm) (Co_3O_4-urea, Co_3O_4-ed, Co_3O_4-NaOH, respectively: 17 mm, 16 mm, and 17 mm). Co_3O_4-urea and Co_3O_4-NaOH exhibited high activity against the Gram-negative *E. aerogenes* (Fig. 9). All three NPs showed higher activity in *C. albicans* than the antifungal. Examining Table 1, it was observed that the cobalt (II, III) oxide (Co_3O_4) NPs prepared in this study recorded high antimicrobial activity similar to the reference drugs

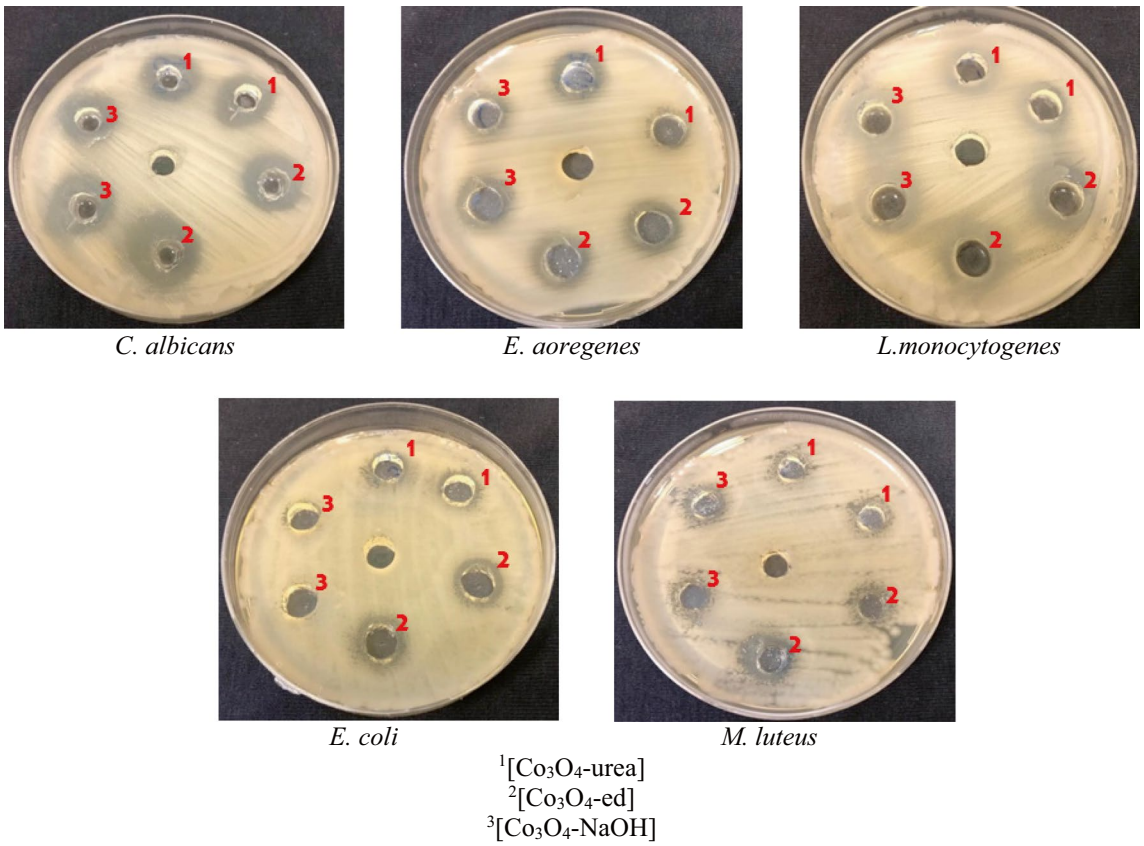

Fig. 7 Antimicrobial activity (inhibition zone [mm]) of Co_3O_4 NPs in Gram(−) and Gram(+) bacteria and yeast

Table 3 Antimicrobial activity of NPs and standard reagents (diameter of zone of inhibition in mm)

		NPs and mean values of zone diameter(mm)			Standard antibiotics				
Microorganisms		Co_3O_4-urea	Co_3O_4-ed	Co_3O_4-NaOH	AMP 10*	SXT 25	AMC 30	K 30	NYS 100
Gr (+)	*M. luteus*	15 I	15 I	14 I	22	21	25	23	N
	S. epidermis	-	-	-	26	25	27	25	N
	S. aureus	-	-	14 I	30	24	30	25	N
	B. cereus	20 H	18 H	19 H	23	25	20	28	N
	L. monocytogenes	13 I	16 I	15 I	28	25	30	26	N
Gr (−)	*P. aeruginosa*	-	-	-	8	18	15	14	N
	K. pneumonia	11 L	18 H	11 L	21	20	21	23	N
	E. aerogenes	17 H	16 I	17 H	21	19	20	24	N
	S. typhi	13 I	13 I	14 I	11	17	19	20	N
	E. coli	17 H	16 I	17 H	10	18	14	25	N
	P. vulgaris	-	11 L	12 I	17	19	20	21	N
Fungi	*C. albicans*	21 H	21 H	22 H	N	N	N	N	20

N not tried, *H* high activity, *I* intermediate activity, *L* low activity.

*Standard reagents: *SXT25* (sulfamethoxazole); *AMP10* (ampicillin); *NYS100* (nystatin); *K30* (kanamycin); *AMC30* (amoxicillin);

used and could be helpful as antimicrobial agents. From the result obtained, it was concluded that these NPs were more effective in Gram(−) than in Gram(+) bacteria. The possible reason for this might be the presence of an external impermeable membrane, a fine peptidoglycan monolayer, and the presence of periplasmic cavity and cell wall composition in Gram(−) bacteria (Graham et al. 2021).

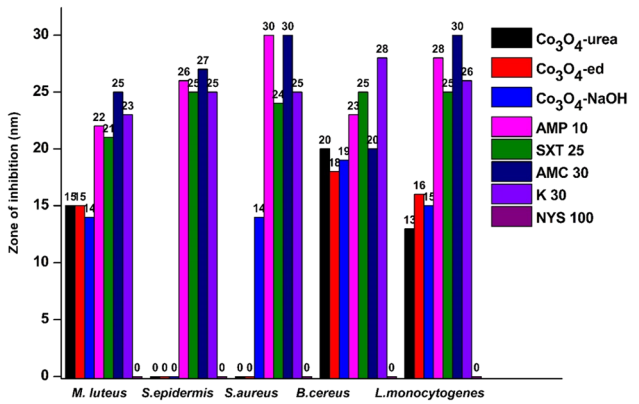

Fig. 8 Graphical illustration of Gram (+) pathogens bacteria (*M. luteus*, *S. epidermis*, *S. aureus*, *B. cereus*, *L. monocytogenes*) and standard reagents

Conclusions

In this study, three Co_3O_4 catalysts with different nanostructured morphologies were produced and their catalytic activities on the reduction of p-NP to p-AP, and on the degradation of MB, were compared. In addition, the effect of morphology on antibacterial properties was investigated. As the Co_3O_4 structures exhibited quite different morphologies, their physical and chemical properties varied greatly, thus exhibiting different catalytic activities and antimicrobial properties. In general, Co_3O_4 structures showed much higher catalytic activities than many metal oxides (such as NiO, Fe_3O_4, ZnO) for p-NP reduction as they have a high surface area and porous nanostructures. Co_3O_4-urea appeared to be the most advantageous for p-NP reduction and completed the reduction of p-NP with $k = 1.86 \times 10^{-2}$ s^{-1} in 270 s. Co_3O_4-urea had a larger surface area, resulting in superior catalytic activity. Likewise, Co_3O_4 structures showed superior performance in the catalytic degradation of MB. In the presence of Co_3O_4-urea catalyst, 98.06% degradation of MB was observed within 60 min. Noble metals are frequently used in such reduction reactions. It shows that Co_3O_4 structures have great potential as non-noble catalysts for practical applications, and they are certainly promising for the reduction of p-NP and MB.

It was determined that Co_3O_4 NPs showed antibacterial and antifungal activities at moderate to good levels against both Gram (+) bacteria, Gram (−) bacteria, and yeast. Co_3O_4-urea showed high activity against *B. cereus*, *E. coli*, and *C. albicans*. In addition, this compound showed the same inhibitory effect as AMC30 (20 mm) for *B. cereus*. It was concluded that these NPs could definitely compete with or even yield better results from commercial antibiotics used in the treatment of microbial infections. For this reason, it is thought that these nanoparticles can be used as a good antimicrobial agent against pathogenic microorganisms or as an additive in antimicrobial products.

Supplementary Information The online version contains supplementary material available at https://doi.org/10.1007/s11356-023-29879-7.

Author contribution N. Kurnaz Yetim carried out the experiments depending on synthesis and characterization of nanoparticles. E. Hasanoğlu Özkan studied the catalytic activities of nanoparticles and wrote the main manuscript text. H. Öğütçü carried out the antimicrobial assessment. Each author contributed to the final manuscript and discussed the findings.

Data availability All data generated or analyzed during this study are included in this article.

Declarations

Ethics approval No ethical issues were violated in this study.

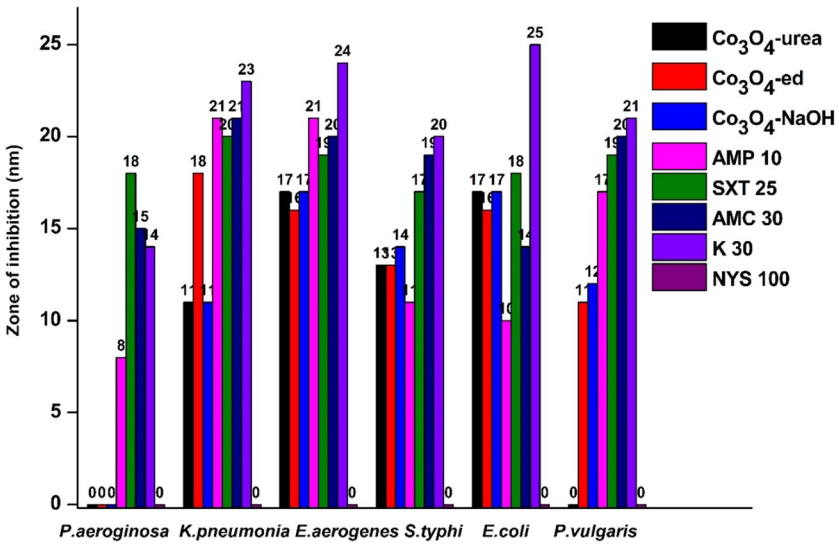

Fig. 9 Graphical illustration of Gram (−) pathogenic bacteria (*P. aeruginosa*, *K. pneumonia*, *E. aerogenes*, *S. typhi*, *E. coli*, and *P. vulgaris*) and standard reagents

Consent to participate All authors agree to participate.

Consent for publication All authors agree for publication.

Conflict of interest The authors declare no competing interests.

References

Abdulhameed AS, Jawad AH, Kashi E, Radzun KA, Al Othman ZA, Wilson LD (2022) Insight into adsorption mechanism, modeling, and desirability function of crystal violet and methylene blue dyes by microalgae: Box-Behnken design application. Algal Res 67:102864. https://doi.org/10.1016/j.algal.2022.102864

Ambika S, Gopinath S, Saravanan K, Sivakumar K, Ragupathi C, Sukantha TA (2019) Structural, morphological and optical properties and solar cell applications of thioglycolic routed nano cobalt oxide material. Energy Rep 5:305–309. https://doi.org/10.1016/j.egyr.2019.02.005

Anar M, Hasanoğlu Özkan E, Ogutcu H, Ağar G, Şakıyan I, Sarı N (2016) Useful agents against Aflatoxin B_1-antibacterial azomethine and Mn(III) complexes involving L-threonine, L-serine, and L-tyrosine. Artif Cells Nanomed Biotechnol 44:853–858. https://doi.org/10.3109/21691401.2014.991792

Anuma S, Mishra P, Bhat BR (2021) Polypyrrole functionalized cobalt oxide graphene (COPYGO) nanocomposite for the efficient removal of dyes and heavy metal pollutants from aqueous effluents. J. Hazard. Mater 416:125929. https://doi.org/10.1016/j.jhazmat.2021.125929

Badruzzaman A, Yuda A, Ashok A, Kumar A (2020) Recent advances in cobalt based heterogeneous catalysts for oxygen evolution reaction. Inorg Chim Acta 511:119854. https://doi.org/10.1016/j.ica.2020.119854

Chen H, Yang M, Tao S, Chen G (2017) Oxygen vacancy enhanced catalytic activity of reduced Co_3O_4 towards p-nitrophenol reduction. Appl Catal B 209:648–656. https://doi.org/10.1016/j.apcatb.2017.03.038

Cheng L, He Y, Gong M, He X, Ning Z, Yu H, Jiao Z (2021) MOF-derived synthesis of Co_3O_4 nanospheres with rich oxygen vacancies for long-term stable and highly selective n-butanol sensing performance. J Alloys Compd 857:158205. https://doi.org/10.1016/j.jallcom.2020.158205

Chiu HY, Wi-Afedzi T, Liu YT, Ghanbari F, Kun-Yi AL (2020) Cobalt oxides with various 3D nanostructured morphologies forc reduction of 4-Nitrophenol: a comparative study. J Water Process Eng 37:101379. https://doi.org/10.1016/j.jwpe.2020.101379

Danish MSS, Bhattacharya A, Stepanova D, Mikhaylov A, Grilli ML, Khosravy M, Senjyu TA (2020) Systematic review of metal oxide applications for energy and environmental sustainability. Metals 10:1604. https://doi.org/10.3390/met10121604

Din MI, Rizwan R, Hussain Z, Khalid R (2021) Biogenic synthesis of mono dispersed Co/CoO nanoparticles using syzygium cumini leaves for catalytic application. Inorg Nano-Met Chem 51(6):773–779. https://doi.org/10.1080/24701556.2020.1808993

Erdogan H (2020) Catalytic degradation of 4-nitrophenol and methylene blue by bioinspired polydopamine coated dipeptide structures. Colloids Interface Sci Commun 39:100331. https://doi.org/10.1016/j.colcom.2020.100331

Fast SA, Gude VG, Truax DD, Martin J, Magbanua BS (2017) A critical evaluation of advanced oxidation processes for emerging contaminants removal. Environ Process 4:283–302. https://doi.org/10.1007/s40710-017-0207-1

Gebre SH, Sendeku MG (2019) New frontiers in the biosynthesis of metal oxide nanoparticles and their environmental applications: an overview. SN Appl Sci 1:928. https://doi.org/10.1007/s42452-019-0931-4

Graham CLB, Newman H, Gillett FN, Smart K, Briggs N, Banzhaf M, Roper DIA (2021) Dynamic network of proteins facilitate cell envelope biogenesis in gram-negative bacteria. Int J Mol Sci 22(23):12831. https://doi.org/10.3390/ijms222312831

Hasanoğlu Ozkan E, Aslan N, Koç MM, Kurnaz Yetim N, Sarı N (2022) Fe_3O_4 nanoparticle decorated novel magnetic metal oxide microcomposites for the catalytic degradation of 4-nitrophenol for wastewater cleaning applications. J Mater Sci: Mater Electron 33:1039–1053. https://doi.org/10.1007/s10854-021-07376-2

He J, Song G, Wang X, Zhou L, Li J (2022) Multifunctional magnetic Fe_3O_4/GO/Ag composite microspheres for SERS detection and catalytic degradation of methylene blue and ciprofloxacin. J Alloys Compd 893:162226. https://doi.org/10.1016/j.jallcom.2021.162226

Jasri K, Abdulhameed AS, Jawad AH, Al Othman ZA, Yousef TA, Al Duaij OK (2023) Mesoporous activated carbon produced from mixed wastes of oil palm frond and palm kernel shell using microwave radiation-assisted K_2CO_3 activation for methylene blue dye removal: Optimization by response surface methodology. Diamond Relat Mater 131:109581. https://doi.org/10.1016/j.diamond.2022.109581

Jeevanandam J, Barhoum A, Chan YS, Dufresne A, Danquah MK (2018) Review on nanoparticles and nanostructured materials: history, sources, toxicity and regulations. Beilstein J Nanotechnol 9:1050–1074. https://doi.org/10.3762/bjnano.9.98

Khan I, Saeed K, Khan I (2019) Nanoparticles: properties, applications and toxicities. Arab J Chem 12(7):908–931. https://doi.org/10.1016/j.arabjc.2017.05.011

Karimi S, Bibak F, Meshkani F, Rastegarpanah A, Deng J, Liu Y, Dai H (2021) Promotional roles of second metals in catalyzing methane decomposition over the Ni-based catalysts for hydrogen production: a critical review. Int J Hydrog Energy 46(39):20435–20480. https://doi.org/10.1016/j.ijhydene.2021.03.160

Kavitha T, Haider S, Kamal T, Ul-Islam M (2017) Thermal decomposition of metal complex precursor as route to the synthesis of Co_3O_4 nanoparticles: antibacterial activity and mechanism. J Alloys Compd 704:296–302. https://doi.org/10.1016/j.jallcom.2017.01.306

Kim HS, Kim HJ, Kim JH, Kim JH, Kang SH, Ryu JH, Park NK, Yun DS, Bae JW (2022) Noble-metal-based catalytic oxidation technology trends for volatile organic compound (VOC) removal. Catalysts 12(63):1–19. https://doi.org/10.3390/catal12010063

Koçoğlu S, Hayvalı Z, Ogutcu H (2021) A polydentate ligand based on 2,2'-dipyridylamine unit linked benzo-15-crown-5; alkali and transition metal complexes; photoresponsive ligand; antimicrobial evaluation against pathogenic microorganisms. Transit Met Chem 46:509–522. https://doi.org/10.1007/s11243-021-00469-1

KurnazYetim N (2021) Hydrothermal synthesis of Co_3O_4 with different morphology: investigation of magnetic and electrochemical properties. J Mol Struct 1226:129414. https://doi.org/10.1016/j.molstruc.2020.129414

Kurnaz Yetim N, Hasanoğlu Özkan E, Akkurt N, Koç MM (2022) Catalytic performance of Fe_3O_4@G2-PAMAM/MoO_3 magnetic nanocomposites for degradation of 4-NP to 4-AP. J Mater Electronic Devices 3(1):1–6

Kurnaz Yetim N, Hasanoğlu Ozkan E (2021) Synthesis of Au-doped magnetic nanocomposites: structural, magnetic, and catalytic properties. J Mater Sci: Mater Electron 32:24766–24774. https://doi.org/10.1007/s10854-021-06922-2

Li Q, Chen Z, Wang H, Yang H, Wen T, Wang S, Hu B, Wang X (2021) Removal of organic compounds by nanoscale zero-valent iron and its composites. Sci Total Environ 792:148546. https://doi.org/10.1016/j.scitotenv.2021.148546

Li Y, Fu Y, Lai C, Qin L, Li B, Liu S, Yi H, Xu F, Li L, Zhang M, Xu M, Duc C, Chen W (2021) Porous materials confining noble metals for the catalytic reduction of nitroaromatics: controllable synthesis and enhanced mechanism. Environ Sci: Nano 8:3067–3097. https://doi.org/10.1039/D1EN00628B

Liu WJ, Wang H, Lee J, Kwon EE, Bui WT, You S, Young-Kwon P, Tong S, Kun-Yi AL (2021) Investigating crystal plane effect of Co_3O_4 with various morphologies on catalytic activation of monopersulfate for degradation of phenol in water. Sep Purif Technol 276:119368. https://doi.org/10.1016/j.seppur.2021.119368

Liu Z, Wang R, Li S, Gu Y, Lan J, Zhou Q, Xu W (2022) Oxygen vacancy-rich ultrafine CoP/Co_3O_4 nanoparticles as high-efficiency trifunctional electrocatalyst. Electrochim Acta 412:140134. https://doi.org/10.1016/j.electacta.2022.140134

Mogudi BM, Ncube P, Meijboom R (2016) Catalytic activity of mesoporous cobalt oxides with controlled porosity and crystallite sizes: evaluation using the reduction of 4-nitrophenol. Appl Catal B 198:74–82. https://doi.org/10.1016/j.apcatb.2016.05.051

Mohanty A, Garg N, Jin RA (2010) Universal approach to the synthesis of noble metal nanodendrites and their catalytic properties. Angew Chem Int Ed 49(29):4962–4966. https://doi.org/10.1002/anie.201000902

Mohd Hanafi NA, Abdulhameed AS, Jawad AH, AL Othman ZA, Yousef TA, Al Duaij OK, Alsaiari NS (2022) Optimized removal process and tailored adsorption mechanism of crystal violet and methylene blue dyes by activated carbon derived from mixed orange peel and watermelon rind using microwave-induced $ZnCl_2$ activation. *Biomass Conv. Biorefi*https://doi.org/10.1007/s13399-022-03646-z

Muhammad I, Kalsoom A, Khan MI, Tahseen K, Khan MA, Asiri AM, Seo J, Khan SB (2019) Pollution, toxicity and carcinogenicity of organic dyes and their catalytic bio- remediation. Curr Pharm Des 25:3653–3671. https://doi.org/10.2174/1381612825666191021142026

Nadhirah Long Tamjid Farki NNA, Abdulhameed AS, Surip SN, Al Othman ZA, Jawad AH (2023) Tropical fruit wastes including durian seeds and rambutan peels as a precursor for producing activated carbon using H_3PO_4-assisted microwave method: RSM-BBD optimization and mechanism for methylene blue dye adsorption. International Journal of Phytoremediationhttps://doi.org/10.1080/152265142175780

Nafiey AA, Addad A, Sieber B, Chastanet G, Barras A, Szunerits S, Boukherroub R (2017) Reduced graphene oxide decorated with Co_3O_4 nanoparticles (rGO-Co_3O_4) nanocomposite: a reusable catalyst for highly efficient reduction of 4-Nitrophenol, and Cr(VI) and dye Removal from aqueous solutions. Chem Eng J 322:375–384. https://doi.org/10.1016/j.cej.2017.04.039

Najafabadi AH, Mansoorianfar M, Liang T, Shahin K, Karimi-Maleh H (2022) A review on magnetic sensors for monitoring of hazardous pollutants in water resources. Sci. Total Environ. 824:153844. https://doi.org/10.1016/j.scitotenv.2022.153844

Najafi M, Azizian S (2020) Catalytic reduction of 4-nitrophenol on the surface of copper/copper oxide nanoparticles: a kinetics study. Appl Nanosci 10:3827–3837. https://doi.org/10.1007/s13204-020-01485-w

Nartop D, Demirel B, Güleç M, HasanogluOzkan E, KurnazYetim N, Sarı N, Ceker S, Ogutcu H, Agar G (2020) Novel polymeric microspheres: synthesis, enzyme immobilization, antimutagenic activity, and antimicrobial evaluation against pathogenic microorganisms. J Biochem Mol Toxicol 34(2):e22432. https://doi.org/10.1002/jbt.22432

Nartop D, Hasanoglu Ozkan E, Gündem M, Ceker S, Agar G, Ogutcu H, Sarı N (2019) Synthesis, antimicrobial and antimutagenic effects of novel polymeric-schiff bases including indol. J Mol Struct 1195:877–882. https://doi.org/10.1016/j.molstruc.2019.06.042

Nartop D, Tokmak E, HasanogluOzkan E, Kızıl HE, Ogutcu H, Agar G, Allı S (2020) Synthesis of novel polymers containing schiff base as potential antimutagenic and antimicrobial agents. J Med Chem Sci 4(3):363–372. https://doi.org/10.26655/jmchemsci.2020.4.6

Naseem T, Durrani T (2021) The role of some important metal oxide nanoparticles for wastewater and antibacterial applications: a review. J Environ Chem Ecotoxicol 3:59–75. https://doi.org/10.1016/j.enceco.2020.12.001

Nava MR, AlvesPereira CA, Brackmann R, Lenzi GG, Dias DT, Ferreirade Souza ÉC, Marcelino Borges JF, Marimonda-Cunha JB, Barreto-Rodrigues M (2022) CeO_2-Fe_2O_3 mixed oxides: Synthesis, characterization and evaluation in the photocatalytic degradation of nitroaromatic compounds from wastewater of the explosives industry. J. Photochem Photobiol A: Chem 428:113839. https://doi.org/10.1016/j.jphotochem.2022.113839

Ogutcu H, Kurnaz Yetim N, Hasanoglu Ozkan E, Eren O, Kaya G, Sarı N, Dıslı A (2017) Nanospheres caped Pt(II) and Pt (IV): synthesis and evaluation as antimicrobial and antifungal Agent. Pol J Chem Technol 19(1):74–80. https://doi.org/10.1515/pjct-2017-0011

Ozkan EH (2023) Detection of 4-nitrophenol in wastewater using microstructures of various morphologies. J Mol Struct 1274(2):134564. https://doi.org/10.1016/j.molstruc.2022.134564

Prakash S, Kumar R, Kumar P, Rani S, Kumari K, Kumari S, Dhakate SR (2022) Reticulated porous carbon foam with cobalt oxide nanoparticles for excellent oxygen evolution reaction. Mater Chem Phys. 275:125131. https://doi.org/10.1016/j.matchemphys.2021.125131

Pugazhendhi A, Vasantharaj S, Sathiyavimal S, Raja RK, Karuppusamy I, Narayanan M, Kandasamy S, Brindhadevi K (2021) Organic and inorganic nanomaterial coatings for the prevention of microbial growth and infections on biotic and abiotic surfaces. Surf Coat Technol 425:127739. https://doi.org/10.1016/j.surfcoat.2021.127739

Rahman A, Jonnalagadda SB (2008) Swift and selective reduction of nitroaromatics to aromatic amines with Ni-boride-silica catalysts system at low temperature. Catal Lett 123:264–268. https://doi.org/10.1007/s10562-008-9417-5

Rajasekar R, Samuel M, Immanuel-Edison TNJ, Raman N (2021) Sustainable synthesis of silver nanoparticles using Alstonia scholaris for enhanced catalytic degradation of methylene blue. J Mol Struct 1246:131208. https://doi.org/10.1016/j.molstruc.2021.131208

Razali NS, Abdulhameed AS, Jawad AH, AlOthman ZA, Yousef TA, Al-Duaij OK, Alsaiari NS (2022) High-surface-area-activated carbon derived from mango peels and seeds wastes via microwave-induced $ZnCl_2$ activation for adsorption of methylene blue dye molecules: statistical optimization and mechanism. Molecules 27:6947. https://doi.org/10.3390/molecules27206947

Ryabchuk P, Agostini G, Pohl MM, Lund H, Agapova A, Junge H, Junge K, Beller M (2018) Intermetallic nickel silicide nanocatalyst-A non-noblemetal-based general hydrogenation catalyst. Sci Adv 4:1–10. https://doi.org/10.1126/sciadv.aat0761

Seitkalieva MM, Samoylenko DE, Lotsman KA, Rodygin KS, Ananikov VP (2021) Metal nanoparticles in ionic liquids: synthesis and catalytic applications. Coord Chem Rev 445:213982. https://doi.org/10.1016/j.ccr.2021.213982

Singh S, Kumar N, Kumar M, Agarwal JA, Mizaikoff B (2017) Electrochemical sensing and remediation of 4-nitrophenol using bio-synthesized copper oxide nanoparticles. Chem Eng J 313:283–292. https://doi.org/10.1016/j.cej.2016.12.049

Sun H, Ahmad M, Zhu J (2013) Morphology-controlled synthesis of Co_3O_4 porous nanostructures for the application as lithium-ion battery electrode. Electrochim Acta 89:199–205. https://doi.org/10.1016/j.electacta.2012.10.116

Wang Z, Zhai S, Lv J, Qi H, Zheng W, Zhai B, An Q (2015) Versatile hierarchical Cu/Fe_3O_4 nanocatalysts for efficient degradation of organic dyes prepared by a facile, controllable hydrothermal

method. RSC Adv 5:74575–74584. https://doi.org/10.1039/c5ra16027h

Wen Y, Zhang J, Xu Q, Wu XT, Zhu QL (2018) Pore surface engineering of metal-organic frameworks for heterogeneous catalysis. Coord Chem Rev 376:248–276. https://doi.org/10.1016/j.ccr.2018.08.012

Xu X, Zhang W, Li Y, Wang P, Zhang Y (2022) Synthesis of Co_3O_4@TiO_2 catalysts for oxygen evolution and oxygen reduction reactions. Microporous Mesoporous Mater 335:111844. https://doi.org/10.1016/j.micromeso.2022.111844

Ye J, Wang S, Li G, He B, Chen X, Cui Y, Zhao W, Sun J (2021) Insight into the morphology-dependent catalytic performance of CuO/CeO_2 produced by tannic acid for efficient hydrogenation of 4-Nitrophenol. Chem Asian J 16(21):3371–3384. https://doi.org/10.1002/asia.202100696

Zaera F (2017) The surface chemistry of metal-based hydrogenation catalysis. ACS Catal 7(8):4947–4967. https://doi.org/10.1021/acscatal.7b01368

Zhang M, Su X, Ma L, Khan A, Wang L, Wang J, Maloletnev AS, Yang C (2021) Promotion effects of halloysite nanotubes on catalytic activity of Co_3O_4 nanoparticles toward reduction of 4-nitrophenol and organic dyes. J Hazard Mater 403:123870. https://doi.org/10.1016/j.jhazmat.2020.123870

Zhang T, He C, Sun F, Ding Y, Wang M, Peng L, Wang J, Lin Y (2017) Co_3O_4 nanoparticles anchored on nitrogen-doped reduced graphene oxide as a multifunctional catalyst for H_2O_2 reduction, oxygen reduction and evolution reaction. Sci Rep 7:43638. https://doi.org/10.1038/srep43638

Zhang Y, Chen Y, Wang T, Zhou J, Zhao Y (2008) Synthesis and magnetic properties of nanoporous Co_3O_4 nanoflowers. Microporous Mesoporous Mater 114:257–261. https://doi.org/10.1016/j.micromeso.2008.01.011